MID-AMERICA TRANSPORTATION CENTER

Report # MATC-MS&T: 124-1

Final Report

WBS: 25-1121-0005-124-1

Interfacial Shear Transfer of Reinforced Concrete with High-Strength Materials

Genda Chen, PhD
Professor and Director
Department of Civil, Architectural, and Environmental Engineering
Missouri University of Science and Technology

Lesley Sneed, PhD
Professor
Department of Civil, Materials, and Environmental Engineering
University of Illinois at Chicago

Tarutal Ghosh Mondal, PhD
Post-Doctoral Fellow

Nikkolas Edgmond
PhD Candidate

2023

A Cooperative Research Project sponsored by
U.S. Department of Transportation- Office of the Assistant Secretary for Research and Technology

MATC

Interfacial Shear Transfer of Reinforced Concrete with High-Strength Materials

Tarutal Ghosh Mondal, Ph.D.
Post-Doctoral Fellow
Civil, Architectural, and Environmental Engineering
Missouri University of Science and Technology

Nikkolas Edgmond
Ph.D. Candidate
Civil, Architectural, and Environmental Engineering
Missouri University of Science and Technology

Lesley Sneed, Ph.D.
Professor
Civil, Materials, and Environmental Engineering
University of Illinois at Chicago

Genda Chen, Ph.D.
Professor and Director
Civil, Architectural, and Environmental Engineering
Center for Intelligent Infrastructure
Missouri University of Science and Technology

A Report on Research Sponsored by

Mid-America Transportation Center

University of Nebraska–Lincoln

July 2023

Technical Report Documentation Page

1. Report No. 25-1121-0005-124-1	2. Government Accession No.	3. Recipient's Catalog No.	
4. Title and Subtitle Interfacial Shear Transfer of Reinforced Concrete with High-Strength Materials		5. Report Date December 2023	
		6. Performing Organization Code	
7. Author(s) Tarutal Ghosh Mondal, Nikkolas Edgmond, Lesley Sneed, Genda Chen		8. Performing Organization Report No. 25-1121-0005-124-1	
9. Performing Organization Name and Address Mid-America Transportation Center Prem S. Paul Research Center at Whittier School 2200 Vine St. Lincoln, NE 68583-0851		10. Work Unit No. (TRAIS)	
		11. Contract or Grant No. 69A3551747107	
12. Sponsoring Agency Name and Address Office of the Assistant Secretary for Research and Technology 1200 New Jersey Ave., SE Washington, D.C. 20590		13. Type of Report and Period Covered January 1, 2011 – December 30, 2023	
		14. Sponsoring Agency Code MATC TRB RiP No. 91994-86	
15. Supplementary Notes			

16. Abstract

Current design provisions pertaining to the shear transfer strength of concrete-to-concrete interfaces, including those of the AASHTO LRFD design specifications and ACI 318 code, are based on limited physical test data from studies conducted decades ago. Since the development of these design provisions, many studies have been conducted to investigate additional parameters. In addition, modern concrete technology has expanded the range of materials available and often includes the use of high-strength concrete and high-strength reinforcing steel. Recent studies examined the applicability of current shear friction design approaches to interfaces that comprise high-strength concrete and/or high-strength steel and identified a need for revision to the existing provisions. To this end, this study leveraged a comprehensive database of test results collected from the literature to propose a deep learning-based predictive model for normal-weight concrete-to-concrete interfacial shear strength. Additionally, a new computation scheme is proposed to estimate the design shear strength with a higher prediction accuracy than the existing AASHTO LRFD and ACI 318 design provisions.

17. ORCID No. of each Researcher Tarutal Ghosh Mondal: 0000-0003-2091-7046 Lesley Sneed: 0000-0003-1528-5611 Genda Chen: 0000-0002-0658-4356	18. Distribution Statement		
19. Security Classif. (of this report) Unclassified	20. Security Classif. (of this page) Unclassified	21. No. of Pages 32	22. Price

Table of Contents

List of Figures iv
List of Tables v
Abstract vii
Chapter 1 Introduction 1
1.1 Background 1
1.2 Research Significance 2
Chapter 2 Existing Design Equations 3
2.1 ACI 318 Building Code Requirements 3
2.2 AASHTO LRFD Bridge Design Specifications 4
2.3 Performance Evaluation 6
Chapter 3 Proposed Neural Network Approach 9
3.1 Prediction of Interfacial Shear Strength 9
3.1.1 Multi-Layer Perceptron 9
3.1.2 Convolutional Neural Network 11
3.1.3 Performance Evaluation 12
3.2 Reduction of the Parameter Space 14
3.3 New Learning-Informed Design (LID) Scheme 18
3.3.1 Neural Additive Models 18
3.3.2 Shape Functions 21
3.3.3 Proposed LID Scheme 23
3.3.4 Illustrative Example 25
3.3.5 Overall Performance 27
Chapter 4 Summary and Conclusions 30
References 31

List of Figures

Figure 2.1 Accuracy of ACI 318 shear friction design provisions with and without prescribed design limits. $vn, test$ and $vn, pred$ denote the experimental and predicted values of interfacial shear strength (in MPa), respectively. NSC, NSS, HSC, and HSS represent normal strength concrete, normal strength steel, high-strength concrete, and high-strength steel, respectively. Concrete having compressive strength greater than 60 MPa is designated herein as HSC. Steel reinforcement having yield strength greater than 420 MPa is identified as HSS. 6.89 MPa = 1 ksi. 6
Figure 2.2 Accuracy of AASHTO LRFD shear friction design provisions with and without prescribed design limits. $vn, test$ and $vn, pred$ denote the experimental and predicted values of interfacial shear strength (in MPa), respectively. NSC, NSS, HSC, and HSS represent normal strength concrete, normal strength steel, high-strength concrete, and high-strength steel, respectively. Concrete having compressive strength greater than 60 MPa is designated herein as HSC. Steel reinforcement having yield strength greater than 420 MPa is identified as HSS. 6.89 MPa = 1 ksi. 8
Figure 3.1 The network architecture of the MLP used for the prediction of interfacial shear strength. The number above each layer denotes the number of neurons in that layer. 10
Figure 3.2 The architecture of 1D CNN used in this study for the prediction of interfacial shear strength. CBR represents a sequence of 1D convolution, batch normalization and rectified linear unit (ReLU) operations. FC denotes a fully connected layer. The feature size at each layer is expressed as a triad in H×W×C format, where H, W, and C denote the height, width, and number of channels, respectively. 11
Figure 3.3 Performance of the proposed deep learning approaches compared to the AASHTO LFRD design provisions. 6.89 MPa = 1 ksi. 13
Figure 3.4 Consequence of parameter reduction and comparison with polynomial regression; The original MLP based on 12 input parameters is denoted by MLP(12). On the other hand, MLP(6) represents a modified MLP based on a reduced set of six parameters. 6.89 MPa = 1 ksi. 16
Figure 3.5 Neural additive models 17
Figure 3.6 The coefficient of determination (R^2) produced by different values of ξ. The plotted values are mean R^2 obtained from a 10-fold cross-validation. 20
Figure 3.7 Feature-specific shape functions. The shape function values are plotted in MPa unit (6.89 MPa = 1 ksi). 21
Figure 3.8 Prediction accuracy of the AASHTO LFRD design equations and the proposed LID scheme in terms of coefficient of determination (R^2), mean absolute error (MAE), and root mean squared error (RMSE). The MAE and RMSE values are plotted in the units of MPa (6.89 MPa = 1 ksi). 28
Figure 3.9 Comparison of the prediction accuracy of the AASHTO LFRD design provisions (with design limits) and the proposed LID scheme (no limits). NSC, NSS, HSC, and HSS represent normal strength concrete, normal strength steel, high-strength concrete, and high-strength steel, respectively. Concrete having compressive strength greater than 60 MPa (9 ksi) is designated herein as HSC. Steel reinforcement having yield strength greater than 420 MPa (60 ksi) is identified herein as HSS. 29

List of Tables

Table 2.1 Coefficients of friction (μ) for normal-weight concrete interfaces as prescribed by ACI 318..... 4
Table 2.2 Maximum vn across the shear plane as prescribed by ACI 318. fc' is the compressive strength of monolithically cast concretes engaged in shear friction. If the concretes on the two sides of the shear interface have different strengths, then the lesser value of fc' should be considered. 4
Table 2.3 Cohesion and friction factors for normal-weight concrete interfaces as prescribed by AASHTO LRFD. For brackets, corbels, and ledges, *c* should be taken as zero..... 5
Table 3.1 The list of parameters used as input to the deep learning models 10
Table 3.2 Minimum and maximum values of the input parameters. 6.89 MPa = 1 ksi. 25.4 mm = 1 in. 20
Table 3.3 Tabular presentation of the parameter-specific shape plots. All shape function values are in MPa unit (6.89 MPa = 1 ksi)..... 24
Table 3.4 A numerical example to illustrate the proposed LID scheme..... 27

Disclaimer

The contents of this report reflect the views of the authors, who are responsible for the facts and the accuracy of the information presented herein. This document is disseminated in the interest of information exchange. The report is funded, partially or entirely, by a grant from the U.S. Department of Transportation's University Transportation Centers Program. However, the U.S. Government assumes no liability for the contents or use thereof.

Abstract

Current design provisions pertaining to the shear transfer strength of concrete-to-concrete interfaces, including those of the AASHTO LRFD design specifications and ACI 318 code, are based on limited physical test data from studies conducted decades ago. Since the development of these design provisions, many studies have been conducted to investigate additional parameters. In addition, modern concrete technology has expanded the range of materials available and often includes the use of high-strength concrete and high-strength reinforcing steel. Recent studies examined the applicability of current shear friction design approaches to interfaces that comprise high-strength concrete and/or high-strength steel and identified a need for revision to the existing provisions. To this end, this study leveraged a comprehensive database of test results collected from the literature to propose a deep learning-based predictive model for normal-weight concrete-to-concrete interfacial shear strength. Additionally, a new computation scheme is proposed to estimate the design shear strength with a higher prediction accuracy than the existing AASHTO LRFD and ACI 318 design provisions.

Chapter 1 Introduction

1.1 Background

The shear friction design concept is applicable in conditions where direct shear must be transferred across a structural concrete plane or interface, such as an existing crack or an interface between dissimilar materials or concretes cast at different times (i.e., construction or cold joint). Shear friction provisions are commonly used in the design of reinforced and precast-prestressed concrete bridge elements/connections, including corbels, dapped double tees, beam bearings, and diaphragms. These types of connections are critical to the safety of the structure because there is little or no redundancy.

The existing shear friction design provisions are largely empirical and are based on physical test data. In fact, the AASHTO LRFD Bridge Design Specifications (AASHTO 2020) and ACI 318 Building Code Requirements for Structural Concrete (ACI-318 2019) use different approaches to compute the shear transfer strength resulting in different shear friction equations and maximum design values. The data used to develop these provisions are predominantly from experiments conducted decades ago. However, modern concrete construction has expanded the range of construction materials available, and recent studies on shear friction have included tests on advanced materials such as high-strength concrete (Kahn and Mitchell 2002), high-performance concrete (Hegger and Görtz, 2003; Crane, 2010), lightweight concrete (Shaw and Sneed, 2014), and high-strength reinforcing steel (Barbosa et al., 2017). Thus, the applicability of the design provisions to interfaces with high-strength concrete and/or high-strength reinforcing steel is worth investigating, especially as these materials become increasingly common in modern bridge and building structures.

1.2 Research Significance

Edgmond and Sneed (2019) assembled a comprehensive database of shear friction test results, enabling an in-depth statistical analysis to evaluate different shear friction design provisions. The authors identified a critical need for revision to current design provisions to ensure safe and cost-effective designs. In this context, the present study proposes a deep learning-based regression model to predict the interfacial shear strength in reinforced concrete. Deep learning has been used in the past to predict the compressive strength (Duan et al. 2013, Dantas et al. 2013), shear strength (Asteris et al. 2019, Bashir and Ashour 2012), and elastic modulus (Demir 2008) of concrete. However, it has not been used to predict the interfacial shear strength at normal-weight concrete-to-concrete interfaces. This study aims to fill this gap by investigating multilayer perceptron (MLP) and one-dimensional convolutional neural network (1D-CNN)-based deep learning models to predict the interfacial shear strength in reinforced concrete based on 12 input parameters. The proposed techniques were observed to outperform the existing design methods that rely on linear expressions as well as the traditional polynomial regression models. This study also went a step further and reduced the dimension of the parameter space from 12 to 6 by an iterative selection, elimination, and grouping of the original parameters. This paved the way for a new design scheme based on a state-of-the-art neural additive modeling approach (Agarwal et al. 2021) that was found to be more accurate than the existing AASHTO LRFD and ACI 318 design provisions. It is believed that the findings of this work will help engender the long-sought changes in the current design provisions leading to safer and more economical design of reinforced concrete structures.

Chapter 2 Existing Design Equations

2.1 ACI 318 Building Code Requirements

The deep learning techniques proposed in this study are benchmarked against the current AASHTO LRFD and ACI 318 design provisions. The ACI 318 code provides a shear friction model that is based on a linear relationship between interfacial normal forces and shear strength that neglects the contribution of concrete cohesion. The ACI 318 code equation for determining the nominal shear strength V_n of a given interface can be written in terms of nominal shear stress v_n as:

$$v_n = \rho f_y(\mu \sin\alpha + \cos\alpha) + \mu\sigma_N \tag{2.1}$$

where v_n is V_n divided by the area of the interface. α is the acute angle between the shear friction reinforcement and the shear interface; the model does not apply if α is greater than 90°. ρ is the ratio of area of shear-friction reinforcement crossing the shear plane to the area of the interface engaged in shear transfer. f_y is the yield strength of shear friction reinforcement [not to exceed 420 MPa (60 ksi)]. μ is the coefficient of interfacial friction as enumerated in Table 2.1. σ_N is the compressive normal stress applied to the shear interface, if present (σ_N is taken as positive for compression). In the case of net tension applied to the interface, a part of the reinforcement crossing the shear plane is utilized in resisting tension and provides no contribution to the shear strength. The residual reinforcement is considered for shear strength estimation as per Equation 2.1 with σ_N taken as zero. The shear strength (v_n) is subject to the maximum limits prescribed by ACI 318 based on the condition of the concrete surface and the compressive strength of concrete

f_c' (Table 2.2). If the concretes on two sides of the shear interface have different strengths, then the lesser value of f_c' should be considered.

Table 2.1 Coefficients of friction (μ) for normal-weight concrete interfaces as prescribed by ACI 318

Contact surface condition	**Coefficient of friction (μ)**
Concrete placed monolithically	1.4
Concrete placed against hardened concrete that is clean, free of laitance, and intentionally roughened to a full amplitude of approximately 6 mm	1.0
Concrete placed against hardened concrete that is clean, free of laitance, and not intentionally roughened	0.6

Table 2.2 Maximum v_n across the shear plane as prescribed by ACI 318. f_c' is the compressive strength of monolithically cast concretes engaged in shear friction. If the concretes on the two sides of the shear interface have different strengths, then the lesser value of f_c' should be considered.

Condition	**Maximum v_n in MPa (ksi)**
Normalweight concrete placed monolithically or placed against hardened concrete intentionally roughened to a full amplitude of approximately 6 mm (1/4 in)	least of $\begin{cases} 0.2f_c' \\ 3.3\ (480) + 0.08f_c' \\ 11\ (1600) \end{cases}$
Other cases	least of $\begin{cases} 0.2f_c' \\ 5.5\ (800) \end{cases}$

2.2 AASHTO LRFD Bridge Design Specifications

Similar to the ACI 318 approach, the AASHTO LRFD model is also based on a linear relationship between interfacial normal forces and shear strength, but it considers an additional component of cohesion, as shown in the following equation written in terms of shear stress:

$$v_n = c + \mu\left(\rho f_y + \sigma_N\right) \tag{2.2}$$

subject to the maximum limit of

$$v_{n,max} = min\{K_1 f_c', K_2\} \tag{2.3}$$

where c is the cohesion factor and K_1, K_2 are friction factors dictated by the interface condition (Table 2.3). For brackets, corbels, and ledges, c should be taken as zero since the effectiveness of cohesion and aggregate interlocking along a vertical crack interface is unreliable. Similar to ACI 318, if the concrete on two sides of the shear interface have different strengths, then the lesser value of f_c' should be considered. It should be noted here that AASHTO LRFD does not specify how to deal with inclined reinforcement. However, the above equation can be extended for the case of inclined reinforcement based on the physical model enunciated in ACI 318. The treatment of the net tension case is identical with the requirements of ACI 318.

Table 2.3 Cohesion and friction factors for normal-weight concrete interfaces as prescribed by AASHTO LRFD. For brackets, corbels, and ledges, *c* should be taken as zero.

Description	**c in MPa (ksi)**	**μ**	**K_1**	**K_2 in MPa (ksi)**
Concrete placed monolithically	2.8 (0.4)	1.4	0.25	10.3 (1.5)
Concrete placed against a clean concrete surface, free of laitance with surface roughened to an amplitude of 6 mm (1/4 in)	1.9 (0.28)	1.0	0.3	12.4 (1.8)
Concrete placed against a clean concrete surface, free of laitance, but not intentionally roughened	0.52 (0.075)	0.6	0.2	5.5 (0.8)

2.3 Performance Evaluation

To evaluate the performance of these design provisions, the database of test results collected by Edgmond and Sneed (2019) was examined. It should be mentioned in this context that some specimens in the original database were subjected to eccentric loading leading to combined bending and shear. The dataset also contained composite beam specimens tested under 3- and 4-point bending configurations. Such loading conditions were beyond the scope of the present study and were therefore eliminated from the revised dataset. Additionally, the database was also comprised of specimens with inclined interfaces, but they were not included in this study. The resulting dataset contained 639 test results.

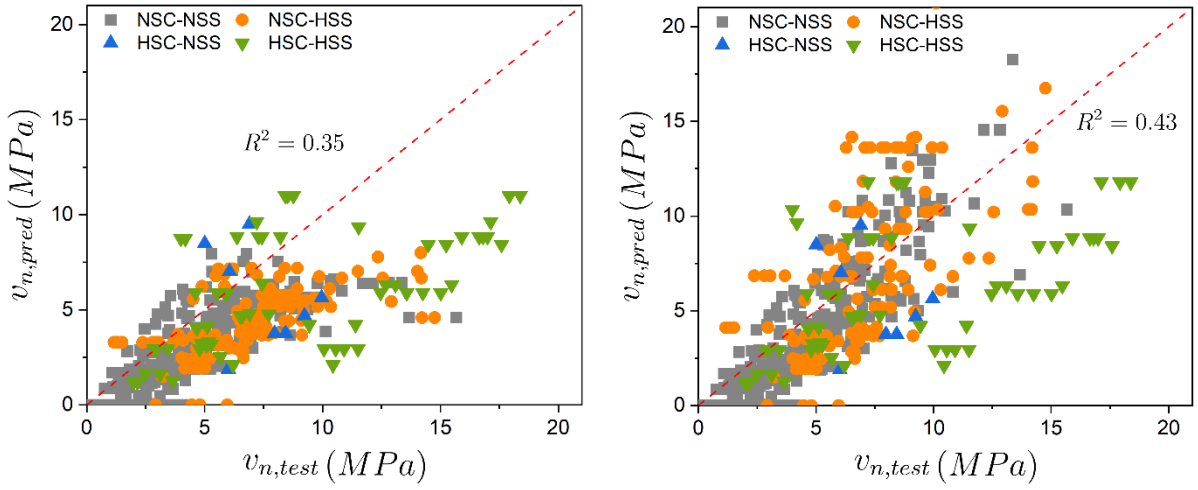

(a) With design limits (b) Without design limits

Figure 2.1 Accuracy of ACI 318 shear friction design provisions with and without prescribed design limits. $v_{n,test}$ and $v_{n,pred}$ denote the experimental and predicted values of interfacial shear strength (in MPa), respectively. NSC, NSS, HSC, and HSS represent normal strength concrete, normal strength steel, high-strength concrete, and high-strength steel, respectively. Concrete having compressive strength greater than 60 MPa is designated herein as HSC. Steel reinforcement having yield strength greater than 420 MPa is identified as HSS. 6.89 MPa = 1 ksi.

The shear strength values calculated by the design provisions are plotted against the test data in Figures 2.1 and 2.2. Load and strength reduction factors are taken as 1.0. It should be noted here that the strength of concrete and reinforcing steel has increased over the years, extending beyond the experimental results on which the design equations were based. The current design specifications get around this by limiting the maximum steel yield strength and maximum nominal shear strength to keep the design within the parameters of the empirical formulas. Therefore, the shear strength values calculated by disregarding the design limits are also plotted in the same figures for comparative evaluations. It was observed the values calculated by AASHTO LRFD ($R^2 = 0.62$) are more accurate than those by ACI 318 ($R^2 = 0.35$) when the design limits are employed. Also, the ACI 318 values tend to be more conservative (i.e., test value is larger than calculated value). These observations can be partly attributed to the fact that the AASHTO LRFD design provision considers the contribution of concrete cohesion, which ACI 318 neglects. As a consequence, ACI 318 predicts zero shear strength for specimens with no shear reinforcement, which is at odds with the experimental observations. The elimination of design limits increased the calculated strength of specimens made of high-strength materials. This is more prominent in specimens with high-strength steel reinforcement, as evident in Figures 2.1 and 2.2. It should be noted concrete with a compressive strength greater than 60 MPa (9 ksi) is designated in this study as high-strength concrete. On the other hand, steel reinforcement having a yield strength greater than 420 MPa (60 ksi) is identified as high-strength steel. Withdrawal of the design limits resulted in an increase in accuracy for ACI 318 but a reduction in accuracy for AASHTO LRFD. For both provisions, it should be noted that removal of design limits resulted in many calculated values being overestimated (i.e., unconservative) by a significant margin. Overall, AASHTO LRFD, along with the prescribed design limits,

produced the most accurate results and is therefore considered as a benchmark to assess the performance of the deep learning techniques introduced later in this paper.

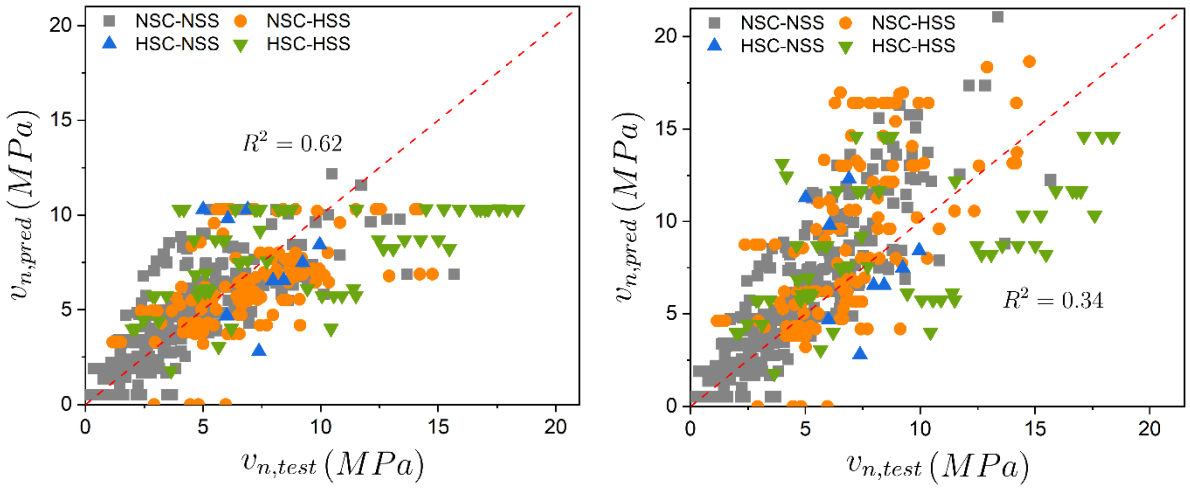

(a) With design limits (b) Without design limits

Figure 2.2 Accuracy of AASHTO LRFD shear friction design provisions with and without prescribed design limits. $v_{n,test}$ and $v_{n,pred}$ denote the experimental and predicted values of interfacial shear strength (in MPa), respectively. NSC, NSS, HSC, and HSS represent normal strength concrete, normal strength steel, high-strength concrete, and high-strength steel, respectively. Concrete having compressive strength greater than 60 MPa is designated herein as HSC. Steel reinforcement having yield strength greater than 420 MPa is identified as HSS. 6.89 MPa = 1 ksi.

Chapter 3 Proposed Neural Network Approach

3.1 Prediction of Interfacial Shear Strength

3.1.1 Multi-Layer Perceptron

To predict the interfacial shear strength, this study examined two classes of deep learning approaches, namely a multi-layer perceptron (MLP) and a 1D convolutional neural network (CNN). An MLP is the simplest form of a neural network consisting of interconnected neurons organized in the form of input, hidden, and output layers (Murtagh 1991). Information flows from the input to the output layer in a feed-forward manner through the connections. The input layer takes in an input, which is subsequently processed by the intermediate hidden layers through a series of linear and nonlinear operations. Finally, the prediction of the neural network is displayed in the output layer. The connections between nodes are characterized by weights learned through a supervised back-propagation training algorithm (Hecht-Nielsen 1992). The input layer in the proposed MLP had 12 nodes corresponding to 12 input parameters, as shown in Table 3.1. It should be noted the interface type (I) was an ordinal variable assuming a value of 1, 2, or 3 for monolithic, intentionally roughened (herein referred to as "rough"), or not intentionally roughened (herein referred to as "smooth") surfaces, respectively. None of the design limits prescribed by the ACI 318 code or the AASHTO LRFD design specifications were put into practice in any of the deep learning-based approaches. It is also worth mentioning many of the parameters listed in Table 3.1 are disregarded by the existing design provisions. The number of nodes in the hidden layers are shown in Figure 3.1. The output layer contained only one node, which corresponded to the interfacial shear strength.

Table 3.1 The list of parameters used as input to the deep learning models

Attribute	Symbol	Parameter
Interface	I	Interface type
	L	Length of shear plane
	W	Width of shear plane
Concrete	f_{c1}, f_{c2}	Experimental compressive strength of concrete on either side of the shear plane
	f_{t1}, f_{t2}	Estimated tensile strength of concrete on either side of the shear plane
Steel	α	Angle of inclination of shear friction reinforcement relative to the shear plane
	n_s	Number of reinforcing bar legs crossing the shear interface
	d	Diameter of reinforcing bars crossing the shear interface
	f_y	Yield strength of shear friction reinforcement
Loading	σ_N	Normal stress applied to the shear interface

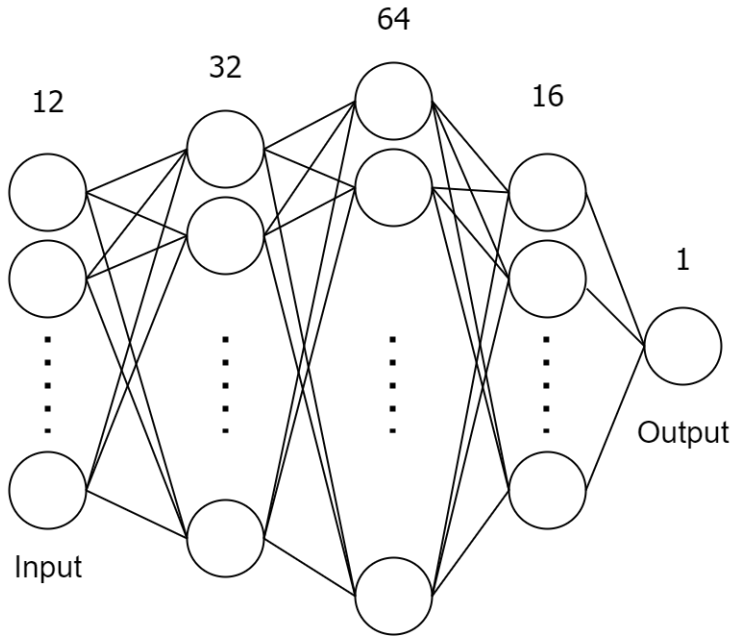

Figure 3.1 The network architecture of the MLP used for the prediction of interfacial shear strength. The number above each layer denotes the number of neurons in that layer.

3.1.2 Convolutional Neural Network

A Convolutional Neural Network (CNN) employs convolution operations to extract spatial features (O'Shea and Nash 2015). In this study, the 12 input parameters were arranged as a 1D array and were passed through a series of convolution, batch normalization, and rectified linear unit (ReLU) layers (Figure 3.2). The output from the last ReLU layer was flattened and was input to a fully connected layer to produce the final network output. In this study, the optimum network parameters were obtained by minimizing the mean squared error between the predicted and target interfacial shear strengths using an Adam-based optimizer (Kingma and Ba 2014).

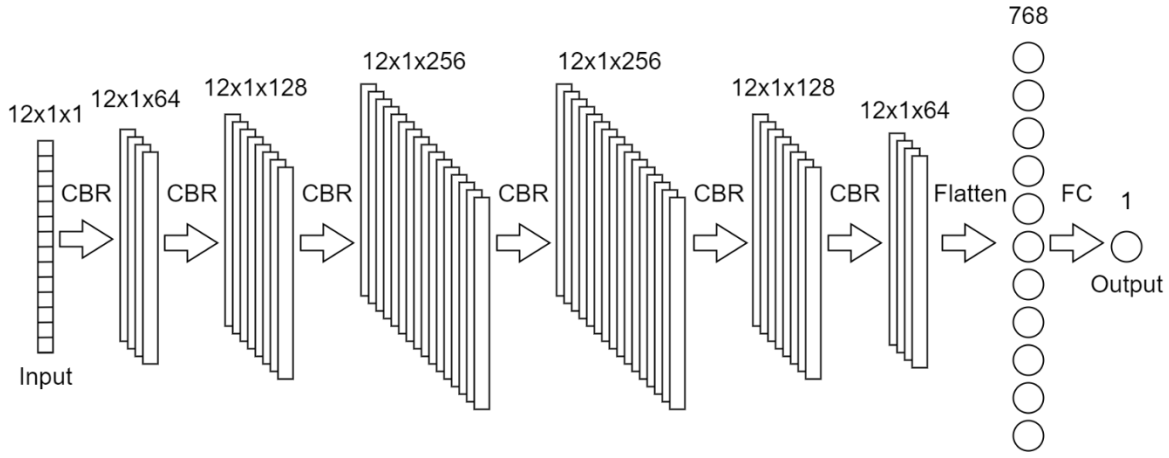

Figure 3.2 The architecture of 1D CNN used in this study for the prediction of interfacial shear strength. CBR represents a sequence of 1D convolution, batch normalization and rectified linear unit (ReLU) operations. FC denotes a fully connected layer. The feature size at each layer is expressed as a triad in H×W×C format, where H, W, and C denote the height, width, and number of channels, respectively.

3.1.3 Performance Evaluation

To assess the performance of the proposed deep learning techniques, three different evaluation metrics were considered in this study, namely the coefficient of determination (R^2), mean absolute error (MAE), and root mean squared error (RMSE). R^2 is the goodness of fit measurement. It is represented by a value ranging from 0 to 1. A value of 1.0 indicates a perfect fit and a highly reliable model, whereas a value of 0 implies that the model utterly fails to fit the data. On the other hand, MAE and RMSE are the two most common indicators used to measure the amount of error in model predictions. A larger value of the metrics means a higher error between the true and predicted values and vice versa.

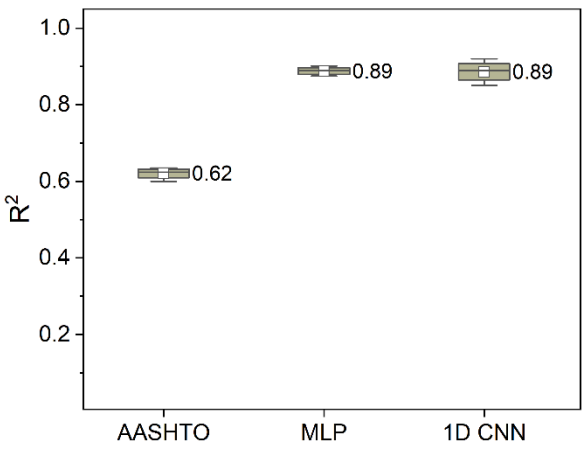

(a) Coefficient of Determination (R^2)

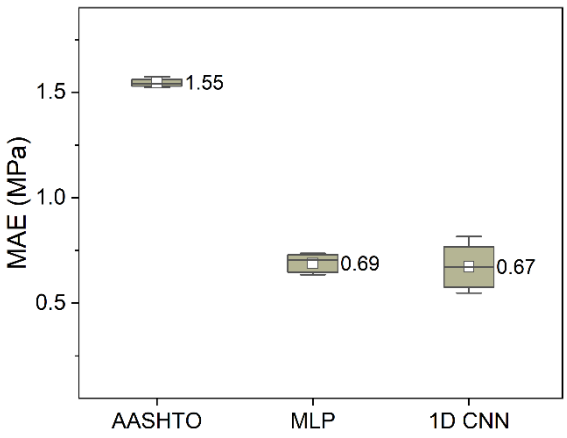

(b) Mean Absolute Error (MAE)

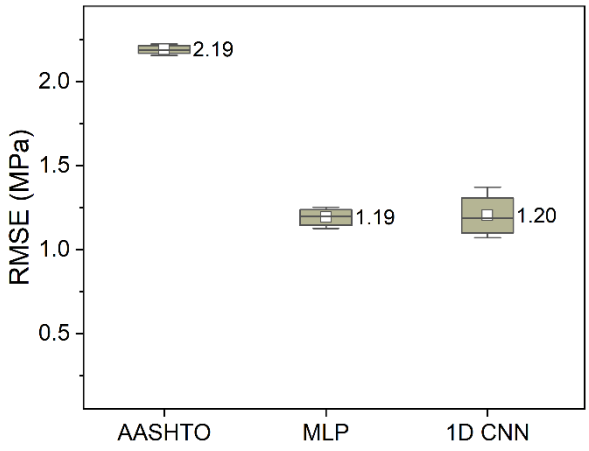

(c) Root Mean Squared Error (RMSE)

Figure 3.3 Performance of the proposed deep learning approaches compared to the AASHTO LFRD design provisions. 6.89 MPa = 1 ksi.

Ten-fold cross-validation was conducted in this study to test the generalization ability of the trained models. At each cross-validation round, 10% of the available data (64) were randomly chosen as the test set, and the remaining 90% of the data (575) were used to train the models. The performance indicators obtained from the cross-validation process are plotted in Figure 3.3. The small squares inside the rectangular boxes represent mean values. The horizontal lines inside the boxes represent the median values. The upper and lower sides of the rectangular

boxes denote one standard deviation on either side of the mean values, and the whiskers protruding out of the boxes represent the minimum and maximum values of the performance metrics. It was observed that the MLP [mean R2: 0.89, mean MAE: 0.69 MPa (0.10 ksi), mean RMSE: 1.19 MPa (0.17 ksi)] outperformed the AASHTO LRFD design specifications by a significantly large margin [mean R2: 0.62, mean MAE: 1.55 MPa (0.22 ksi), mean RMSE: 2.19 MPa (0.32 ksi)]. The 1D CNN exhibited a similar accuracy to the MLP [mean R2: 0.89, mean MAE: 0.67 MPa (0.10 ksi), mean RMSE: 1.20 MPa (0.17 ksi)]. However, the predictions of the MLP were more robust than the 1D CNN, as indicated by the height of the corresponding rectangular boxes. Thus, the MLP is identified to be more suitable than the 1D CNN-based approach and is used for all subsequent analyses. The inclusion of a broader range of parameters and the inherent ability of deep learning-based techniques to model nonlinear relations can be credited for the overall superiority of these methods compared to the existing provisions that were developed based on the evaluation of discrete sets of test data.

3.2 Reduction of the Parameter Space

Despite the proven advantage, deep learning-based prediction models, unfortunately, have very few takers among structural engineers and designers. Therefore, it is improbable that these advanced modeling techniques will replace the prevailing design provisions anytime soon. Therefore, this study seeks to propose a new design scheme by striking a delicate balance between the accuracy of deep learning models and the intuitive simplicity and physical understanding of the existing design models. As a steppingstone towards that objective, this section aims to reduce the dimension of the parameter space, which will be instrumental in enhancing the model's simplicity. Subsequent to this, a recent advancement in deep learning is

leveraged to propose a simple computation scheme as a more accurate alternative to the existing design provisions.

Backed by the physical understanding of the underlying principles, this study achieved a reduced parameter set by the iterative selection, elimination, and aggregation from the original list of parameters. At the end of the process, six key parameters are produced, indicating a 50% reduction in the parameter space dimension:

$$x_1 = I \tag{3.1}$$

$$x_2 = LW \tag{3.2}$$

$$x_3 = \sqrt{min(f_{c1}, f_{c2})} \tag{3.3}$$

$$x_4 = \frac{\pi d^2 n_s}{4LW} f_y \tag{3.4}$$

$$x_5 = \alpha \tag{3.5}$$

$$x_6 = \sigma_N \tag{3.6}$$

It was observed that the reduction in the number of parameters slightly reduced the prediction accuracy of the MLP (Figure 3.4). It produced a mean R2 of 0.85, mean MAE of 0.83 MPa (0.12 ksi), and mean RMSE of 1.33 MPa (0.19 ksi), indicating a slight reduction in performance compared to the original 12-parameter model [mean R2: 0.89, mean MAE: 0.69 MPa (0.10 ksi), mean RMSE: 1.19 MPa (0.17 ksi)].

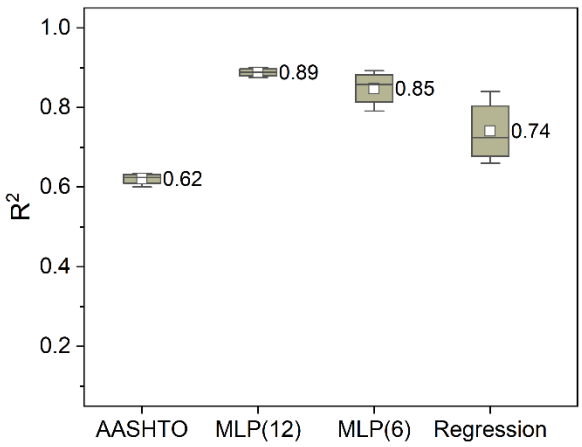

(a) Coefficient of Determination (R^2)

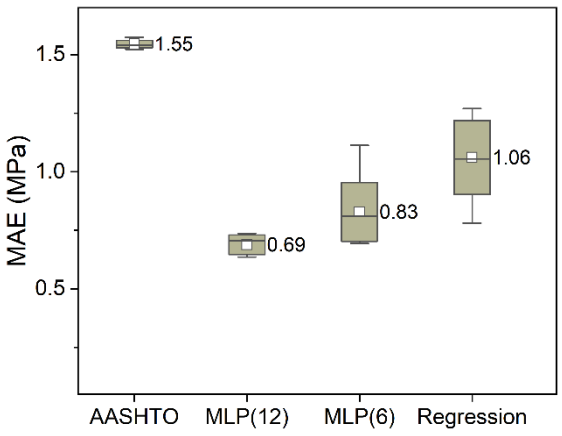

(b) Mean Absolute Error (MAE)

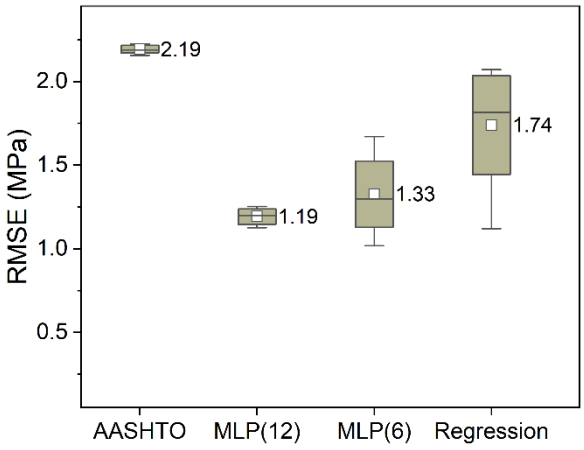

(c) Root Mean Squared Error (RMSE)

Figure 3.4 Consequence of parameter reduction and comparison with polynomial regression; The original MLP based on 12 input parameters is denoted by MLP(12). On the other hand, MLP(6) represents a modified MLP based on a reduced set of six parameters. 6.89 MPa = 1 ksi.

Further, this study tested the efficacy of an ordinary polynomial regression model, which was based on a feature space that comprised all polynomial combinations of the parameters with a degree less than or equal to a specified degree. The highest specified degree of the polynomial features varied sequentially, and quadratic features produced the most accurate predictions [mean R2: 0.74, mean MAE: 1.06 MPa (0.15 ksi), mean RMSE: 1.74 MPa (0.25 ksi)]. Although the

quadratic regression model considerably outperformed the design equation provided by the AASHTO LRFD specification [mean R2: 0.62, mean MAE: 1.55 MPa (0.22 ksi), mean RMSE: 2.19 MPa (0.32 ksi)], it still did not perform as well as the MLP-based algorithm. This confirms the point that the traditional regression models are no match for the latest deep learning-based techniques, particularly when accuracy is a key objective. On the whole, this signifies an important breakthrough that sets the stage for developing a new design scheme, as presented in the following section.

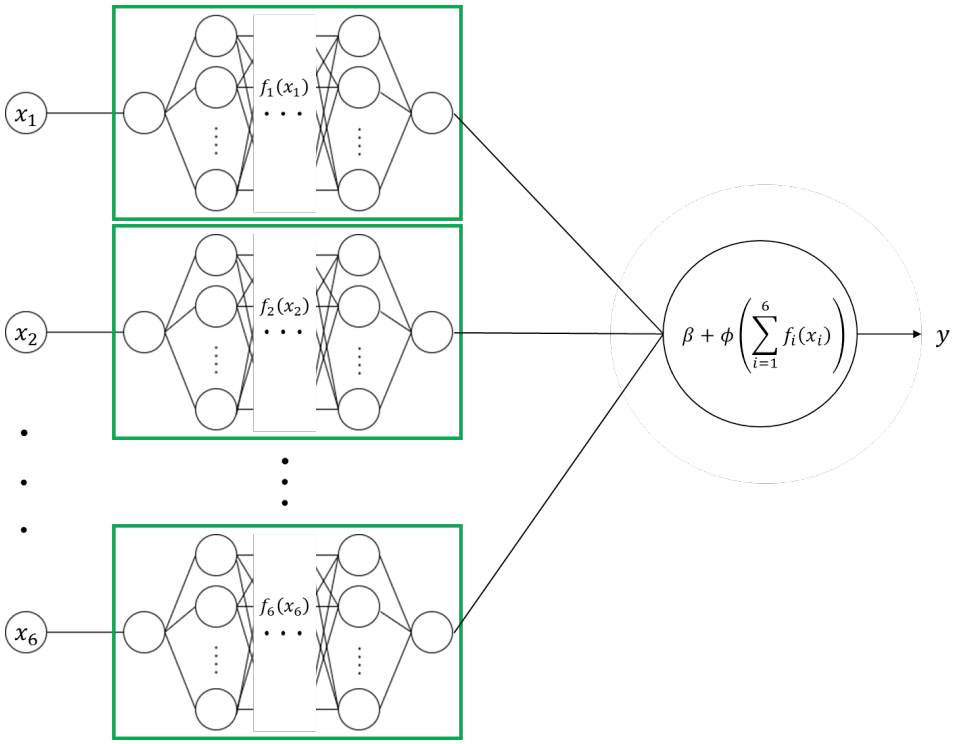

Figure 3.5 Neural additive models

3.3 New Learning-Informed Design (LID) Scheme

3.3.1 Neural Additive Models

This section is dedicated to the development of a new LID scheme which is accurate and straightforward. To this end, this study leveraged a recent development in deep learning called neural additive models (Agarwal et al. 2021). This additive modeling approach jointly trains a set of neural networks that attend to a single input parameter (Figure 3.5). This study used six MLP blocks to handle the six input parameters identified in the previous section. The MLP blocks, apart from the input and output layers, contain three intermediate layers, comprising 16 neurons each. The MLP blocks can learn arbitrary complex shape functions, a combination of which produce the final model outputs, as shown in the following equation.

$$y = \beta + \phi(s) \tag{3.8}$$

Where

$$s = \sum_{i=1}^{6} f_i(\bar{x}_i) \tag{3.9}$$

$$\begin{aligned} \phi(s) &= \xi s + \frac{1-\xi}{\bar{y}^2} s^3, \qquad \xi \in [0,1] \\ &= \frac{-\xi}{\bar{y}^4} s^5 + \frac{1+\xi}{\bar{y}^2} s^3, \qquad \xi \in [-1,0] \end{aligned} \tag{3.10}$$

$\bar{x}_1, \bar{x}_2, \ldots, \bar{x}_6$ are normalized parameters given by

$$\bar{x}_i = \frac{x_i - x_{i,min}}{x_{i,max} - x_{i,min}} \tag{3.11}$$

$x_{i,max}$ and $x_{i,min}$ are the maximum and minimum values for the i-th parameter as enumerated in Table 3.2. $\bar{y}$ is the mean value of observed shear strength. ξ is a coefficient that regulates the mix proportion of linear and non-linear terms. To estimate the optimum value of ξ, its value is increased gradually from -1 to 1. For each increment it increases by, the ξ value is followed by a training of the model using 10-fold cross-validation. The mean R^2 values obtained from 10 rounds of cross-validation are plotted in Figure 3.6 against the corresponding ξ values. When $\xi = 0$, $\phi(s)$ is a cubic function of s. When $0 < \xi < 1$, $\phi(s)$ contains both linear and cubic terms. $\xi = 1$ gives rise to an entirely linear function of s. In the same token, $\phi(s)$ is an amalgam of cubic and quintic terms for $-1 < \xi < 0$. Lastly, $\xi = -1$ indicates a pure quintic function of s. Figure 3.6 reveals that the best performance is achieved when $\xi = 0$, implying that $\phi(s)$ is a cubic function of s. It can be mentioned in this context that a non-linear function of s enables an interaction among various shape function components, which is otherwise nonviable in traditional additive modeling approaches where the shape functions are linearly combined. Therefore, a cubic $\phi(s)$ is chosen in this study for all subsequent analyses.

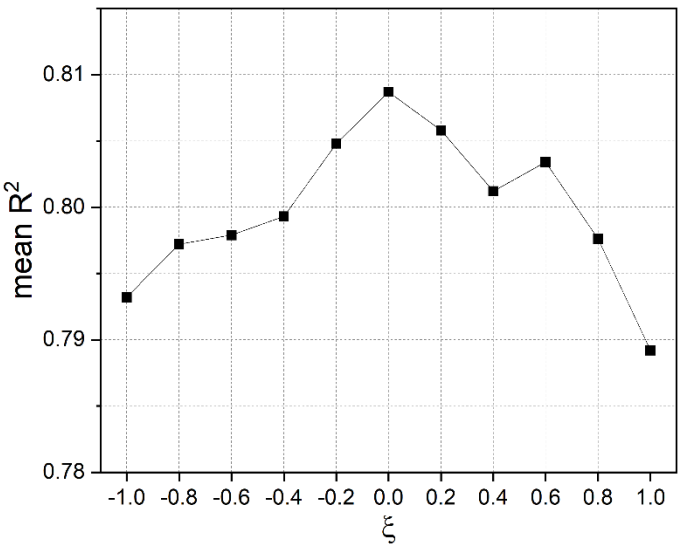

Figure 3.6 The coefficient of determination (R^2) produced by different values of ξ. The plotted values are mean R^2 obtained from a 10-fold cross-validation.

Table 3.2 Minimum and maximum values of the input parameters. 6.89 MPa = 1 ksi. 25.4 mm = 1 in.

x_i	x_1	x_2 (mm^2)	x_3 ($\sqrt{\text{MPa}}$)	x_4 (MPa)	x_5 (°)	x_6 (MPa)
$x_{i,min}$	1	20645.12	3.86	0.00	0.00	-2.76
$x_{i,max}$	3	247741.44	10.67	15.18	135.00	10.34

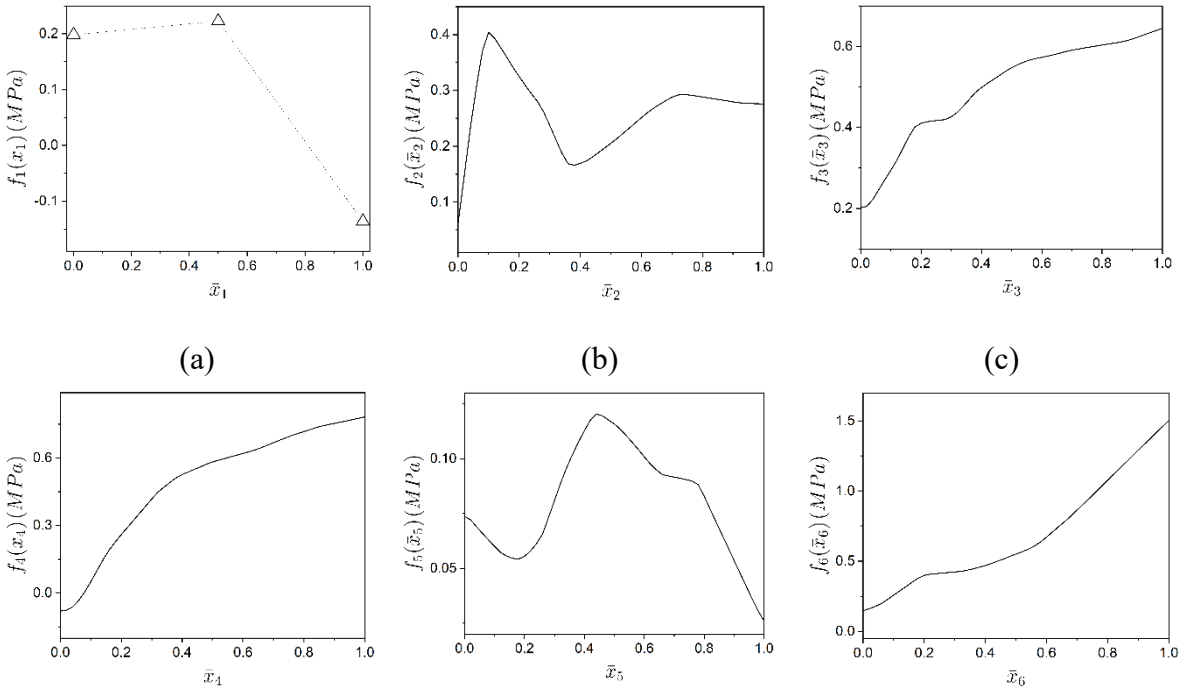

Figure 3.7 Feature-specific shape functions. The shape function values are plotted in MPa unit (6.89 MPa = 1 ksi).

3.3.2 Shape Functions

Once the training is complete, the shape functions can be plotted against the respective normalized parameter values. Each parameter produces 10 shape functions, corresponding to 10 cross-validation rounds. These shape functions are averaged to obtain a single shape function corresponding to each parameter.

$$f_i(\bar{x}_i) = \frac{1}{10}\sum_{j=1}^{10} f_i^{\,j}(\bar{x}_i) \tag{3.12}$$

where $f_i^j(\bar{x}_i)$ denotes the shape function for the i-th parameter produced by the j-th cross-validation round. w_j is the coefficient of determination (R^2) on the test set corresponding to the j-th cross-validation round. $f_i(\bar{x}_i)$ is the final aggregated shape function for the i-th parameter, as plotted in Figure 3.7. x_1 is assigned an integer that can only be equal to one, two, or three, which correspond to $\bar{x}_1$ of zero, 0.5, and one, respectively; thus, other values of this parameter are meaningless.

These shape functions are largely consistent with the physical understanding of the problem. As per classical shear friction theory and recently developed models (Palieraki et al., 2021; Palieraki et al., 2022), direct shear across a concrete-to-concrete interface is resisted by a combination of three mechanisms (cohesion, friction, and dowel action), which are affected by different parameters. These mechanisms do not reach their maximum contributions simultaneously, which adds to the complexity of the problem. Experimental evidence has shown that one of the important parameters that influences shear transfer is surface roughness (Saemann and Washa, 1964). A smoother surface leads to less aggregate interlocking and cohesion, resulting in reduced shear strength. This behavior is reflected in Figure 3.7(a), where a significant dip in the shape plot was noticed for smooth surfaces. Another parameter that plays a major role in interfacial shear transfer is the concrete compressive strength. Previous studies have established that an increase in the concrete compressive strength results in an increase in the interfacial shear strength (Mattock and Hawkins, 1972; Shaw and Sneed, 2014), which is corroborated by the behavior depicted in Figure 3.7(c). The figure also exhibits a softening effect towards the right, which is indicative of a diminishing return on increasing compressive strength. The clamping stress, which is defined as the product of the ratio and yield strength of shear reinforcement, is also known to significantly impact the interfacial shear strength (Saemann and

Washa, 1964; Hofbeck et al., 1969; Bass et al., 1989; Echegaray-Oviedo et al., 2014). It restrains crack dilation, develops aggregate interlocking, and thereby contributes positively to shear transfer strength through friction and dowel action. This is substantiated by the positive correlation exhibited in Figure 3.7(d). The figure also exhibits a softening effect towards the right, which is indicative of a diminishing return on increasing reinforcement ratio, yield strength, or both. Previous studies have indicated the presence of an external normal compressive stress can have an additive effect on the clamping stress leading to an enhanced shear friction strength (Mattock and Hawkins, 1972). On the other hand, the presence of an external normal tensile stress is seen to reduce the interfacial shear strength (Chatterjee, 1971). The observations in Figure 3.7(f) are in sync with this prior knowledge, facilitating the physical interpretation of the shape function plot. Interestingly, the behavior in Figure 3.7(b) suggests there is no consistent correlation between the interfacial area and shear strength. However, further investigation is needed to see whether size effects the different shear resisting mechanisms or interfacial shear strength.

3.3.3 Proposed LID Scheme

The shape functions can also be presented in a tabular form, as shown in Table 3.3. This tabular presentation of shape plots forms the basis of the proposed LID scheme. To predict the interfacial shear strength of an interface, the known parameter values are first normalized according to Equation 3.11. The shape function value corresponding to each normalized parameter is then interpolated from the two nearest entries in Table 3.3. In the end, all the estimated shape function values are combined to compute the interfacial shear strength ($\hat{y}$), as follows:

$$\hat{y} = \beta + \left(\sum_{i=1}^{6} \hat{f}_i(\bar{x}_i) \right)^3 \tag{3.13}$$

$$\beta = 0.02 \tag{3.14}$$

where $\hat{f}_i(\bar{x}_i)$ is the interpolated shape function value corresponding to parameter i. β is the bias term evaluated by an averaging technique analogous to that shown in Equation 3.12.

Table 3.3 Tabular presentation of the parameter-specific shape plots. All shape function values are in MPa unit (6.89 MPa = 1 ksi).

$\bar{x}$	$f_1(\bar{x}_1)$	$f_2(\bar{x}_2)$	$f_3(\bar{x}_3)$	$f_4(\bar{x}_4)$	$f_5(\bar{x}_5)$	$f_6(\bar{x}_6)$
0.00	0.20	0.06	0.20	-0.08	0.07	0.15
0.02		0.15	0.21	-0.08	0.07	0.16
0.04		0.23	0.22	-0.06	0.07	0.18
0.06		0.31	0.25	-0.03	0.07	0.20
0.08		0.37	0.27	0.00	0.06	0.23
0.10		0.40	0.29	0.05	0.06	0.26
0.12		0.39	0.32	0.10	0.06	0.29
0.14		0.38	0.35	0.15	0.06	0.32
0.16		0.36	0.38	0.19	0.05	0.35
0.18		0.34	0.40	0.23	0.05	0.38
0.20		0.33	0.41	0.26	0.06	0.40
0.22		0.31	0.41	0.29	0.06	0.41
0.24		0.29	0.42	0.32	0.06	0.41
0.26		0.28	0.42	0.35	0.07	0.42
0.28		0.26	0.42	0.39	0.07	0.42
0.30		0.24	0.43	0.42	0.08	0.42
0.32		0.21	0.44	0.45	0.09	0.43
0.34		0.19	0.45	0.47	0.10	0.44
0.36		0.17	0.47	0.49	0.10	0.45
0.38		0.17	0.49	0.51	0.11	0.46
0.40		0.17	0.50	0.53	0.11	0.47
0.42		0.17	0.51	0.54	0.12	0.48
0.44		0.18	0.52	0.55	0.12	0.50
0.46		0.19	0.53	0.56	0.12	0.52
0.48		0.20	0.54	0.57	0.12	0.53
0.50	0.22	0.21	0.55	0.58	0.12	0.55

$\bar{x}$	$f_1(\bar{x}_1)$	$f_2(\bar{x}_2)$	$f_3(\bar{x}_3)$	$f_4(\bar{x}_4)$	$f_5(\bar{x}_5)$	$f_6(\bar{x}_6)$
0.52		0.21	0.55	0.59	0.11	0.57
0.54		0.22	0.56	0.60	0.11	0.59
0.56		0.23	0.57	0.61	0.11	0.61
0.58		0.24	0.57	0.61	0.10	0.64
0.60		0.25	0.57	0.62	0.10	0.67
0.62		0.26	0.58	0.63	0.10	0.71
0.64		0.27	0.58	0.64	0.09	0.75
0.66		0.28	0.58	0.65	0.09	0.78
0.68		0.28	0.59	0.66	0.09	0.82
0.70		0.29	0.59	0.67	0.09	0.86
0.72		0.29	0.59	0.68	0.09	0.91
0.74		0.29	0.60	0.69	0.09	0.95
0.76		0.29	0.60	0.70	0.09	0.99
0.78		0.29	0.60	0.71	0.09	1.03
0.80		0.29	0.60	0.72	0.08	1.08
0.82		0.29	0.61	0.73	0.08	1.12
0.84		0.28	0.61	0.73	0.07	1.16
0.86		0.28	0.61	0.74	0.07	1.21
0.88		0.28	0.61	0.75	0.06	1.25
0.90		0.28	0.62	0.75	0.05	1.29
0.92		0.28	0.62	0.76	0.05	1.33
0.94		0.28	0.63	0.76	0.04	1.38
0.96		0.28	0.63	0.77	0.04	1.42
0.98		0.28	0.64	0.78	0.03	1.46
1.00	-0.14	0.28	0.64	0.78	0.03	1.50

3.3.4 Illustrative Example

The proposed LID scheme can be illustrated with the help of an example. Consider specimen BRS12-4 from Hanson (1960). The specimen has a rough interface that is 304.8 mm (12.0 in) long and 203.2 mm (8.0 in) wide. The compressive strengths of concrete on either side of the shear interface are 21.7 and 26.7 MPa (3.1 and 3.9 ksi). Interfacial reinforcement in the form of two 12.7 mm (0.5 in) diameter bars with a yield strength of 352 MPa (51 ksi) is oriented orthogonal to the interface. No compressive stress is applied normal to the interface. Accordingly, let

$$x = [2, 304.80, 203.20, 4.66, 1.44, 90, 0] \tag{3.15}$$

be a set of parameters characterizing a shear interface under investigation. Normalization of the parameters as per Equation 3.11 results in

$$\bar{x} = [0.50, 0.18, 0.12, 0.09, 0.67, 0.21] \tag{3.16}$$

Now, for $\bar{x}_1 = 0.50$, $\bar{x}_2 = 0.18$, and $\bar{x}_3 = 0.12$, the shape function values $\hat{f}_1(\bar{x}_1)$, $\hat{f}_2(\bar{x}_2)$, and $\hat{f}_3(\bar{x}_3)$ can be read directly from Table 3.3 as $\hat{f}_1(\bar{x}_1) = 0.22$, $\hat{f}_2(\bar{x}_2) = 0.34$, and $\hat{f}_3(\bar{x}_3) = 0.32$. Next, to estimate the shape function value corresponding to $\bar{x}_4 = 0.09$, the two nearest neighbors in the lookup table are identified as $u = 0.08$ and $v = 0.10$. The corresponding shape function values are $f_4(u) = 0.00$ and $f_4(v) = 0.05$. Therefore, $\hat{f}_4(\bar{x}_4)$ can be computed by employing a simple linear interpolation as:

$$\hat{f}_4(\bar{x}_4) = f_4(u) + \big(f_4(v) - f_4(u)\big) \times \frac{\bar{x}_4 - u}{v - u} \tag{3.17}$$

This leads to $\hat{f}_4(\bar{x}_4) = 0.03$. In the same manner, the other shape function values can be estimated as shown in Table 3.4. Finally, these shape function values can be combined per Equation 3.13, resulting in an estimated interfacial strength of 2.79 MPa (0.40 ksi). This estimated shear strength compares favorably with (within 13.88% of) the test result of 2.45 MPa (0.36 ksi) (Hanson, 1960). The AASHTO LRFD design provisions predict a shear strength of 3.34 MPa (0.48 ksi) for this specimen (36.33% larger than the test value), which is far less accurate than the proposed LID scheme.

Table 3.4 A numerical example to illustrate the proposed LID scheme

$\bar{x}_i$	u	v	$f_i(u)$	$f_i(v)$	$\hat{f}_i(\bar{x}_i)$	$v_{n,LID}$	$v_{n,AASHTO}$	$v_{n,test}$
$\bar{x}_1$ = 0.50	0.50	0.50	0.22	0.22	0.22			
$\bar{x}_2$ = 0.18	0.18	0.18	0.34	0.34	0.34			
$\bar{x}_3$ = 0.12	0.12	0.12	0.32	0.32	0.32	2.79	3.34	2.45
$\bar{x}_4$ = 0.09	0.08	0.10	0.00	0.05	0.03	(13.88%)	(36.33%)	
$\bar{x}_5$ = 0.67	0.66	0.68	0.09	0.09	0.09			
$\bar{x}_6$ = 0.21	0.20	0.22	0.40	0.41	0.405			

Note: $\bar{x}_i$ indicates the normalized value of parameter i . u and v signify the normalized parameter values corresponding to two nearest entries in Table 3.3. The corresponding shape function values are represented as $f_i(u)$ and $f_i(v)$, respectively. $\hat{f}_i(\bar{x}_i)$ implies the shape function value obtained by linear interpolation of the nearest entries. $v_{n,LID}$ denotes the interfacial shear strength estimated by the proposed LID scheme as per Equation 3.13. $v_{n,AASHTO}$ connotes the shear strength predicted by AASHTO LRFD design equations. The experimental shear strength for the specimen under consideration is symbolized by $v_{n,test}$. All shear strength values are reported in MPa unit (6.89 MPa = 1 ksi). The values inside ( ) indicate the percentage errors relative to the experimental result.

3.3.5 Overall Performance

The interfacial shear strength is obtained for all specimens in the data set. The accuracy of the predicted values is compared with the AASHTO LRFD design specifications in terms of R^2, MAE, and RMSE in Figure 3.8. The proposed LID scheme produces significantly higher R^2 (0.79) and lower MAE [1.09 MPa (0.16 ksi)] and RMSE [1.61 MPa (0.23 ksi)] values compared to the AASHTO LRFD design specification [R2: 0.62, MAE: 1.55 MPa (0.22 ksi), RMSE: 2.19 MPa (0.32 ksi)]. The estimated interfacial shear strength values are plotted against the experimental observations in Figure 3.9, which indicates a much closer correlation with the proposed LID scheme than the AASHTO LRFD design provision. It is also observed that the relative superiority of the proposed LID scheme cuts across normal and high-strength materials. This is a considerable advancement in which structural engineers and designers can use for a more accurate prediction of the interfacial shear strength leading to a safer and more economical design of reinforced concrete members. However, there are still some unconservative predictions, particularly for specimens with high-strength concrete and high-strength steel.

Therefore, future studies should aim to further reduce the extent of overestimation to address the needs of a conservative design paradigm.

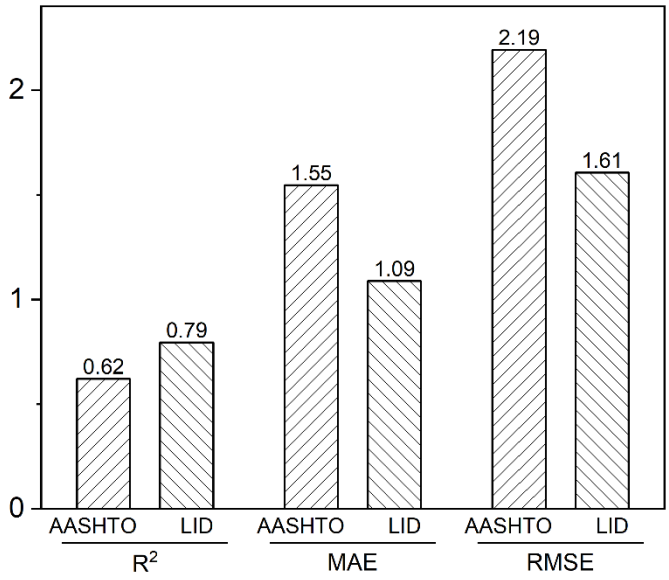

Figure 3.8 Prediction accuracy of the AASHTO LFRD design equations and the proposed LID scheme in terms of coefficient of determination (R^2), mean absolute error (MAE), and root mean squared error (RMSE). The MAE and RMSE values are plotted in the units of MPa (6.89 MPa = 1 ksi).

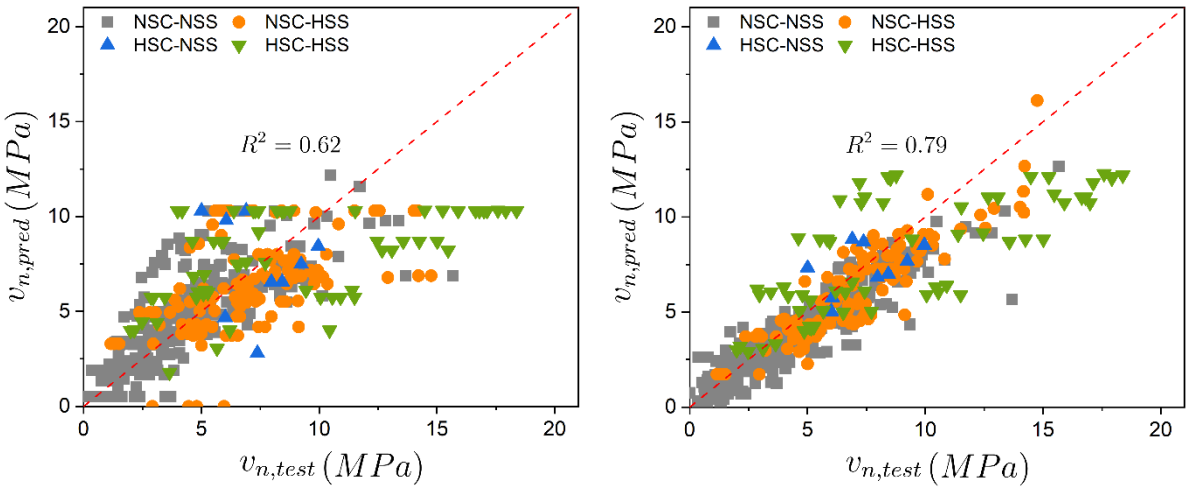

(a) AASHTO LRFD (b) Proposed LID scheme

Figure 3.9 Comparison of the prediction accuracy of the AASHTO LFRD design provisions (with design limits) and the proposed LID scheme (no limits). NSC, NSS, HSC, and HSS represent normal strength concrete, normal strength steel, high-strength concrete, and high-strength steel, respectively. Concrete having compressive strength greater than 60 MPa (9 ksi) is designated herein as HSC. Steel reinforcement having yield strength greater than 420 MPa (60 ksi) is identified herein as HSS.

Chapter 4 Summary and Conclusions

This study identified the inaccuracy of the existing design provisions vis-à-vis the prediction of shear strength at the normal-weight concrete-to-concrete interface. Two deep learning models based on MLP and 1D CNN were explored for a more accurate prediction of the interfacial shear strength. The proposed MLP, which is more robust than the 1D CNN, was observed to considerably outperform both the AASHTO LRFD and ACI 318 design provisions. This is attributable to a neural network's superior ability to learn nonlinear functions. Subsequently, a neural additive model was leveraged to develop a novel LID scheme based on a reduced parameter space. The proposed LID scheme outperformed the existing design equations by considerable margins. The effectiveness of any learning-based method relies on the quality of data used to train the model. In this study, to ensure reliable predictions, ten-fold cross-validation was conducted by splitting the data into different train-test sets. The model's ability to perform well on both the training and test sets indicates that it can generalize well to novel, unseen data without being overly influenced by potentially noisy training data. Overall, it is believed that this study will motivate the design community to consider such tools to help update the existing design provisions to benefit from some of the clear advantages the latest deep learning techniques can offer.

This study did not account for the interplay between different design parameters, which is a scope for future work. Future studies should also look into a more granular gradation of the interface, taking into account the amplitude of roughness, aggregate properties, presence of a pre-existing crack along the shear plane, and the time gap between the casting of the adjacent surfaces. Moreover, quantifying the uncertainty and reliability of the predicted shear strength values is another important research area that merits attention.

References

AASHTO (2020), "AASHTO LRFD Bridge Design Specifications," American Association of State Highway and Transportation Officials (AASHTO), Washington, DC., Standard 9th Edition, 2020.

ACI 318 (2019), "Building Code Requirements for Structural Concrete (ACI 318-14) and Commentary (ACI 318R-19)," American Concrete Institute (ACI), Farmington Hills, MI, Standard, 2019.

Agarwal, R., Melnick, L., Frosst, N., Zhang, X., Lengerich, B., Caruana, R., and Hinton, G. E. "Neural additive models: Interpretable machine learning with neural nets," *Advances in Neural Information Processing Systems*, vol. 34, pp. 4699–4711, 2021.

Asteris, P. G., Armaghani, D. J., Hatzigeorgiou, G. D., Karayannis, C. G., and Pilakoutas, K. "Predicting the shear strength of reinforced concrete beams using artificial neural networks," *Computers and Concrete, An International Journal*, vol. 24, no. 5, pp. 469–488, 2019.

Barbosa, A. R., Trejo, D., and Nielson, D. "Effect of high-strength reinforcement steel on shear friction behavior," *Journal of Bridge Engineering*, vol. 22, no. 8, p. 04017038, 2017.

Bashir, R. and Ashour, A. "Neural network modelling for shear strength of concrete members reinforced with frp bars," *Composites Part B: Engineering*, vol. 43, no. 8, pp. 3198–3207, 2012.

Bass, R. A., Carrasquillo, R. L., and Jirsa, J. O. "Shear transfer across new and existing concrete interfaces," *Structural Journal*, vol. 86, no. 4, pp. 383–393, 1989.

Chatterjee, P. "Shear transfer in reinforced concrete," 1971.

Crane, C. K. *Shear and shear friction of ultra-high performance concrete bridge girders*. Georgia Institute of Technology, 2010.

Dantas, A. T. A., Leite, M. B., and Nagahama, K. de Jesus. "Prediction of compressive strength of concrete containing construction and demolition waste using artificial neural networks," *Construction and Building Materials*, vol. 38, pp. 717–722, 2013.

Demir, F. "Prediction of elastic modulus of normal and high strength concrete by artificial neural networks," *Construction and building Materials*, vol. 22, no. 7, pp. 1428–1435, 2008.

Duan, Z.-H., Kou, S.-C., and Poon, C.-S. "Prediction of compressive strength of recycled aggregate concrete using artificial neural networks," *Construction and Building Materials*, vol. 40, pp. 1200– 1206, 2013.

Edgmond, N. J. and Sneed, L. H. "Examination of shear friction design provisions," Pre-

cast/Prestressed Concrete Institute (PCI), Chicago, IL, Tech. Rep. pp. 147, 2019.

Echegaray-Oviedo, J., Cuenca, E., Navarro-Gregori, J., and Serna, P. “Influence of the fiber reinforcement in concrete under direct shear,” in *10th fib International PhD Symposium in Civil Engineering Proceedings*, 2014, pp. 415–424.

Hanson, N. W. *Precast-prestressed concrete bridges: 2. Horizontal shear connections*. Portland Cement Association, Research and Development Laboratories Skokie, 1960.

Hecht-Nielsen, R. “Theory of the backpropagation neural network,” in *Neural networks for perception*. Elsevier, 1992, pp. 65–93.

Hegger, J. and Görtz, S. Nachträglich ergänzte Querschnitte mit horizontaler Fuge nach DIN 1045 - 1. Beton - und Stahlbetonbau, 98(5), pp.277-284, 2003

Hofbeck, J., Ibrahim, I., and Mattock, A. H. “Shear transfer in reinforced concrete,” in *Journal Proceedings*, vol. 66, no. 2, 1969, pp. 119–128.

Kahn, L. F. and Mitchell, A. D. “Shear friction tests with high-strength concrete,” *Structural Journal*, vol. 99, no. 1, pp. 98–103, 2002.

Kingma, D. P. and Ba, J. “Adam: A method for stochastic optimization,” *arXiv preprint arXiv:1412.6980*, 2014.

Mattock, A. H. and Hawkins, N. M. “Shear transfer in reinforced concrete—recent research,” *PCI Journal*, vol. 17, no. 2, pp. 55–75, 1972.

Murtagh, F. “Multilayer perceptrons for classification and regression,” *Neurocomputing*, vol. 2, no. 5-6, pp. 183–197, 1991.

O’Shea, K. and Nash, R. “An introduction to convolutional neural networks,” *arXiv preprint arXiv:1511.08458*, 2015.

Palieraki, V., Vintzileou, E., and Silva, J. F. “Interface shear strength under monotonic and cyclic loading.” *ACI Structural Journal*, vol. 119, no. 3, 2022.

Palieraki, V., Vintzileou, E., and Silva, J. “Behavior of RC interfaces subjected to shear: State-of-the art review,” *Construction and Building Materials*, vol. 306, p. 124855, 2021.

Saemann, J. and Washa, G. W. “Horizontal shear connections between precast beams and cast-in-place,” in *Journal Proceedings*, vol. 61, no. 11, 1964, pp. 1383–1410.

Shaw, D. M. and Sneed, L. H. “Interface shear transfer of lightweight-aggregate concretes cast at different times.” *PCI Journal*, vol. 59, no. 3, 2014.